ms to 100 ms. This ended up with a sample irradiated through a matrix of dots, which had many internal connectivity issues. The homogeneity of the material was not good, and the porosity and material quality were not optimized to the level presented in the previous section.

In any case, it set the foundations and helped the team develop standard technologies, such as the use of gel electrolytes, which were translated to the following experiments. The choice of aqueous based electrolyte has already been discussed, as this type of electrolyte was easy to handle within the lab facilities available. Within this type, acidic, neutral or basic electrolytes could be fabricated. The most common ones for their use in supercapacitors have been acidic electrolytes, which the group was using since many years ago and presented high ionic conductivity. Among acidic electrolytes, due to its prevalence in the literature and easy availability, two solutions have been tested, namely sulfuric acid (H_2SO_4) and phosphoric acid (H_3PO_4).

Figure 27 presents a direct comparison of the CV curves of identical UV-LIG microsupercapacitors assembled with different electrolytes. As seen in Figure 27a, sulfuric acid clearly outperforms phosphoric acid when used as a liquid electrolyte in microsupercapacitors, probably due to the better availability of ions in the solution, being sulphuric acid a stronger acid. On the other hand, the tilted shape of those CV curves indicate that the fabricated UV-LIG material presents a high resistance, which ESR has been measured to be in the order of 1000 ohms.

When assembling these devices, the disadvantages of using a liquid electrolyte have already been mentioned, being contact corrosion, electrolyte leakage, high degradation, and poor durability, leading in the end to safety issues. This is why new electrolytes based on gels were proposed. After confirming the viability of the gelation process based on [183], polyvinyl alcohol (PVA) was selected as the gel agent. Several tests were made to settle on a specific PVA gel, as many different types are available commercially. Finally, PVA 86-89% hydrolyzed, of medium molecular weight, was selected due to its easy solution in liquids. 1 gram of PVA, in small beads which could be grinded in a mortar, was mixed into 10 mL of acidic solution (1 to 10 ratio). After constant stirring and gentle heating at 85^{o}C for 2h, the electrolyte became transparent and of a viscous texture.

Figure 27b shows the cyclic voltammetry measurements performed in UV-LIG supercapacitors assembled using gel electrolytes of both acidic solutions. The behaviour is the same as before, sulfuric acid allowing for better performance,

although the shape of the C-V curve, slightly more tilted than before hints at a higher resistance, expected by the gel-nature of the electrolyte.

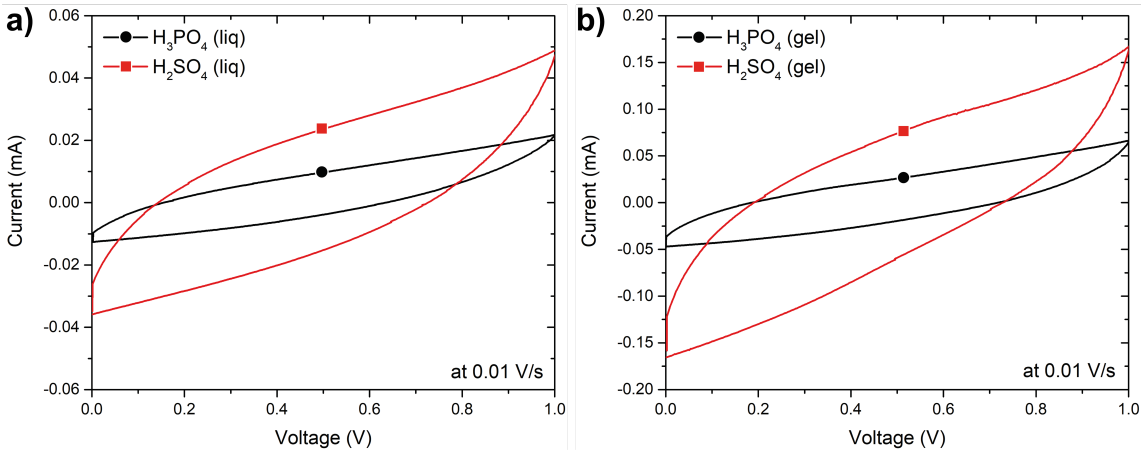

Figure 27: Cyclic voltammetry comparison of two aqueous electrolytes, 1M H_2SO_4 and 1M H_3PO_4 in liquid and in gel, in UV-LIG MSCs. (a) Comparison of liquid electrolytes at 0.01 V/s scan rate. (b) Comparison of gel electrolytes at 0.01 V/s scan rate. Symbols have been added for accessibility purposes only.

Finally, to assemble the supercapacitor devices using this new gel electrolyte, a small vacuum step had to be introduced to help the electrolyte penetrate in the small pores of the LIG material. Gel infiltration into porous carbon electrodes is an essential part of supercapacitor assembly using gel-based electrolytes [184], [185].

4.2.2. LIG microsupercapacitors in aqueous gel electrolyte

To test the electrochemical performance of the fabricated devices, several techniques have been used, including cyclic voltammetry, galvanostatic charge-discharge and electrochemical impedance spectroscopy. As the goal is not to only characterize the full device, but to indirectly benchmark the potential of the different LIG materials for its application in supercapacitors, several devices of each laser condition have been fabricated. The measurements have been performed in a two-electrode configuration without using a reference electrode due to the limitations imposed by the geometry of the devices and the nature of the electrolyte.

In Figure 28, a comparison of the four selected samples is shown. Using cyclic voltammetry, a technique where the voltage of the device is swept through the entire operational voltage window, in this case 0 to 1 volt, the current needed to reach each voltage state is recorded. The shape of the CV response for an ideal supercapacitor would be a squared plot, symmetric around the x axis, with constant current while charging and discharging, and with an amplitude as high as possible, indicating a

bigger capacitance. For Figure 28a, the cyclic voltammetry at 0.02 V/s scan rate of the four samples show that S-2.0-45 is the most capacitive sample, being the one reaching higher currents. While all samples show a sloped plot shape, due to a non-negligible electrode resistance, sample S-1.8-25 is by far the most resistive.

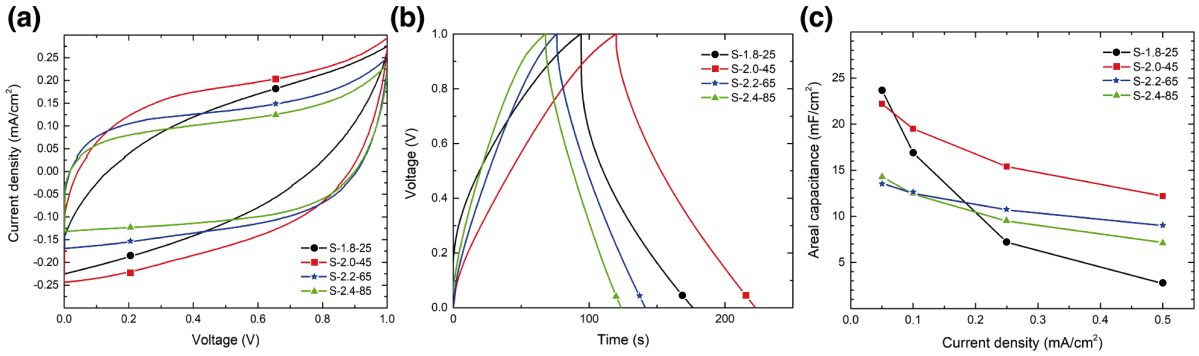

Figure 28: Electrochemical performance of the fabricated MSCs at different laser conditions in PVA gel electrolyte, 1M H_2SO_4. (a) Cyclic voltammetry comparison (CV) graphs of the four selected MSCs at a 0.02 V/s scan rate. b) Galvanostatic charge-discharge of the four selected samples at 0.1 mA/cm² current density. (c) Areal capacitance of the four different samples calculated from the GCD as a function of the current density. Symbols have been added for accessibility purposes only.

In Figure 28b, the same behaviour is tested but through a galvanostatic charge-discharge measurement, which instead of forcing a voltage through the device, now introduces or extracts a fixed current, measuring the change in voltage. This technique gives the same information as the previous CV, but is more similar to the real usage of the device. Again, S-2.0-45 is the one that, charging at 0.1 mA/cm², takes longer to charge and discharge, hinting to a higher capacitance. For an ideal supercapacitor this measurement will yield a triangular graph, and the quick drop in voltage after changing the current polarity is directly related to the equivalent series resistance (ESR) of the device (equation 2.2). S-1.8-25, as in the previous case, show a higher ESR and a poor, more curved discharge profile.

Finally, Figure 28c condenses all areal capacitance values for the four selected samples at a series of discharge current densities, extracted using equation 2.3. With this analyzed data, it is clear that the best sample is S-2.0-45, which keeps high areal capacitance for higher current densities. Only at the slowest discharge condition, S-1.8-25 overperforms it, but it quickly drops for higher currents. The complete CV and GCD graphs of all mentioned samples are shown in Figure 29 and Figure 30, including S-1.8-25, S-2.0-45, S-2.2-65 and S-2.4-85, plus the remaining fabricated samples S-1.8-40, S-2.0-60, S-2.2-80 and S-2.4-70.

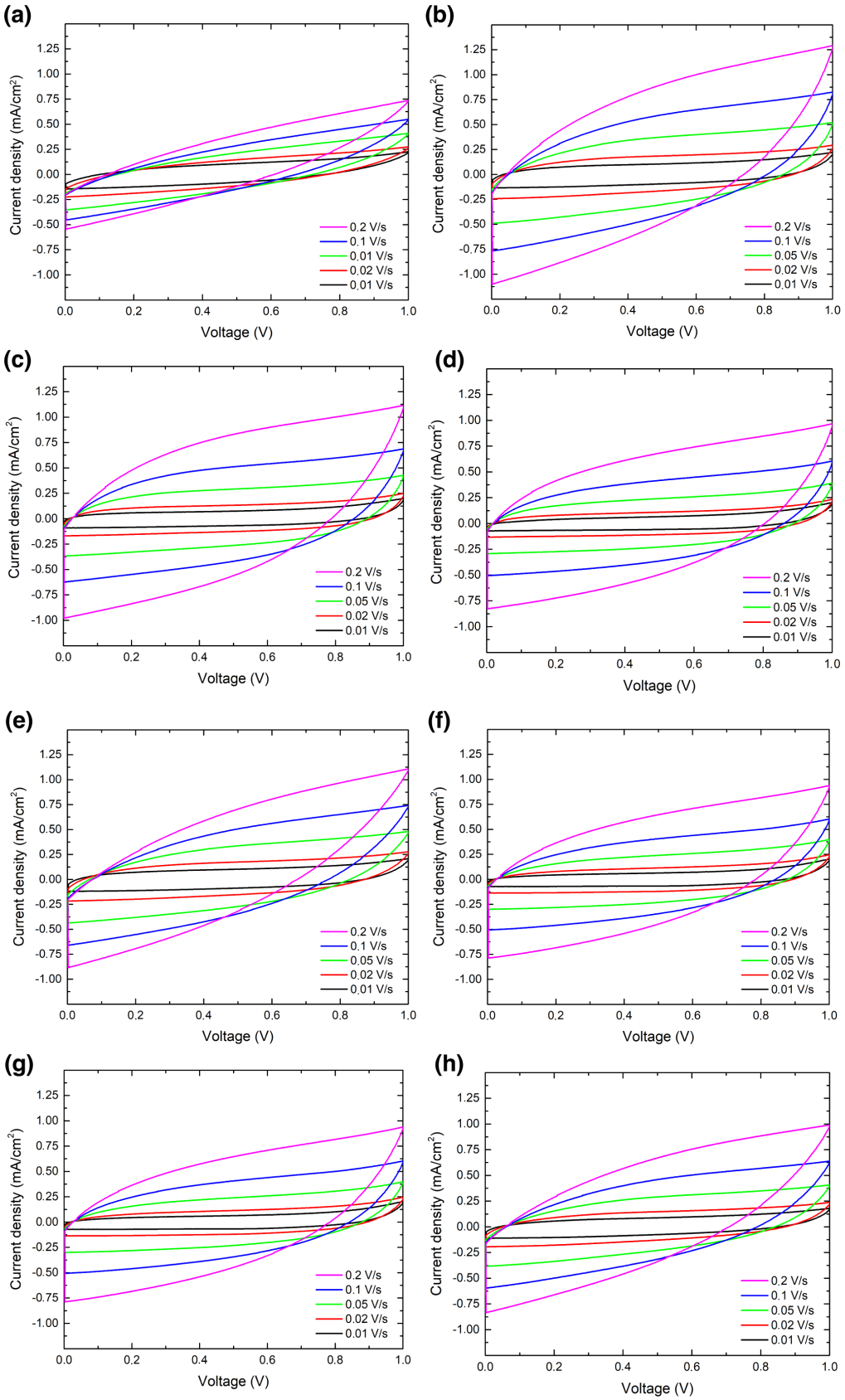

Figure 29: Cyclic voltammetry graphs of all samples at different scan speeds, from 0,01 V/s to 0,2 V/s. (a) S-1.8-25, (b) S-2.0-45, (c) S-2.2-65, (d) S-2.4-85, (e) S-1.8-40, (f) S-2.0-60, (g) S-2.2-80, (h) S-2.4-70

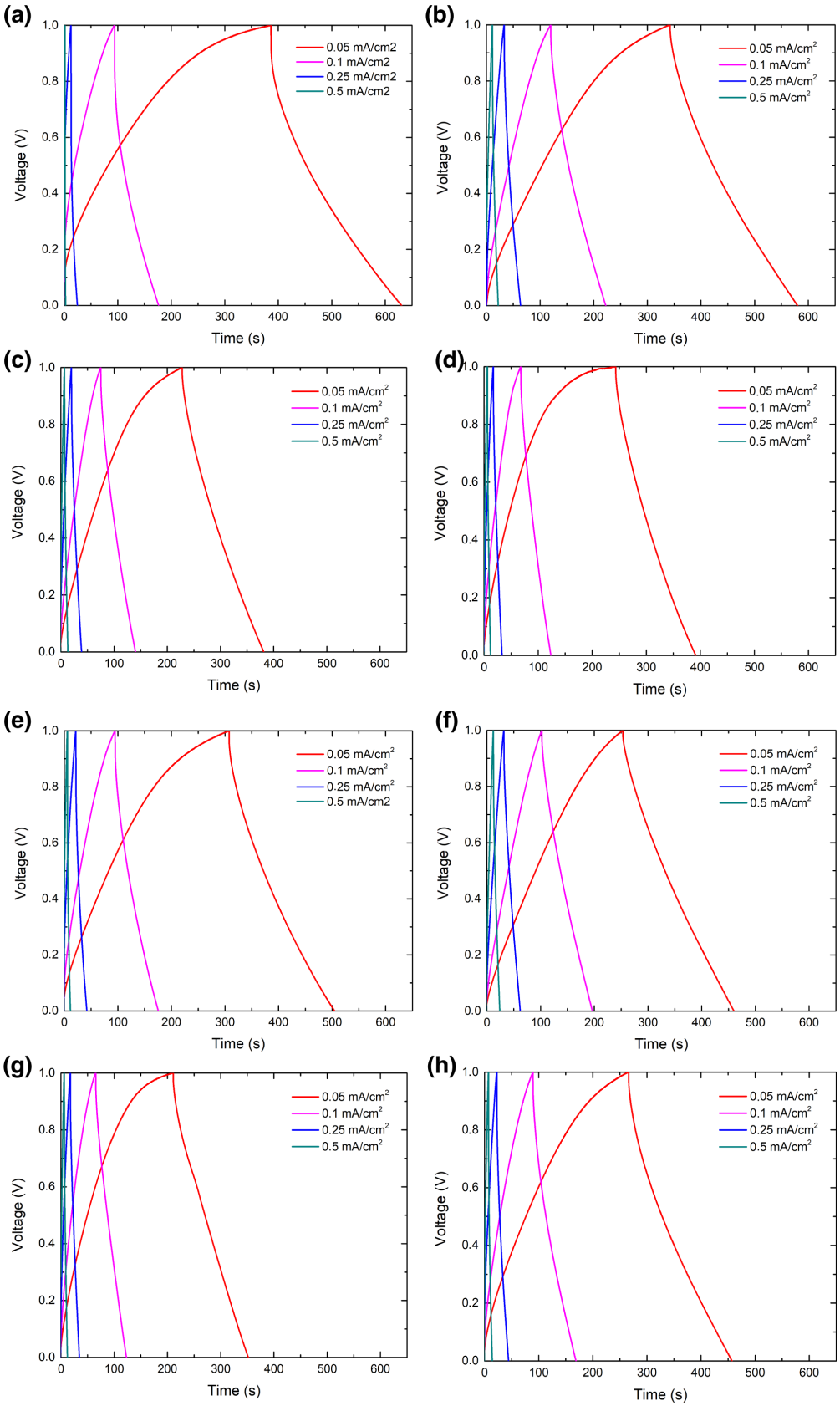

Figure 30: Galvanostatic charge-discharge graphs of all samples at different current densities, from 0,05 mA/cm² to 0,5 mA/cm². (a) S-1,8-25, (b) S-2,0-45, (c) S-2,2-65, (d) S-2,4-85, (e) S-1,8-40, (f) S-2,0-60, (g) S-2,2-80, (h) S-2,4-70.

An important technique for characterising supercapacitors is Electrochemical Impedance Spectroscopy, briefly introduced in section 2.2.3. This measurement can give precious information about the tested device. It introduces to the device a small AC potential, which gives back an AC current signal, typically shifted in phase. The most common plot to represent an EIS measurement is the Nyquist plot, with the real part of the impedance (Z') in the x-axis, and the negative imaginary part of the impedance (Z'') in the y-axis. By fitting the impedance response to the one given by a parametric equivalent circuit, the behaviour of the supercapacitor can be modelled by a simple circuit.

Without describing in much detail this technique, which is very complex and has not been a central part of this work, a simplified reading of the main supercapacitor metrics can be done as indicated in Figure 31a. All four EIS measurements are shown in Figure 31b. The y=0 value, the crossing with the x-axis represents the electrode resistance, with S-2.0-45 having the best value of 58 Ω. For all cases but S-1.8-25, the electrolyte resistance is very small, and similarly happens for the diffuse layer resistance. Also, the three best performing samples present a steep slope at low frequencies, representative of a capacitance produced by the electric double layer, and not dependant on ion diffusion.

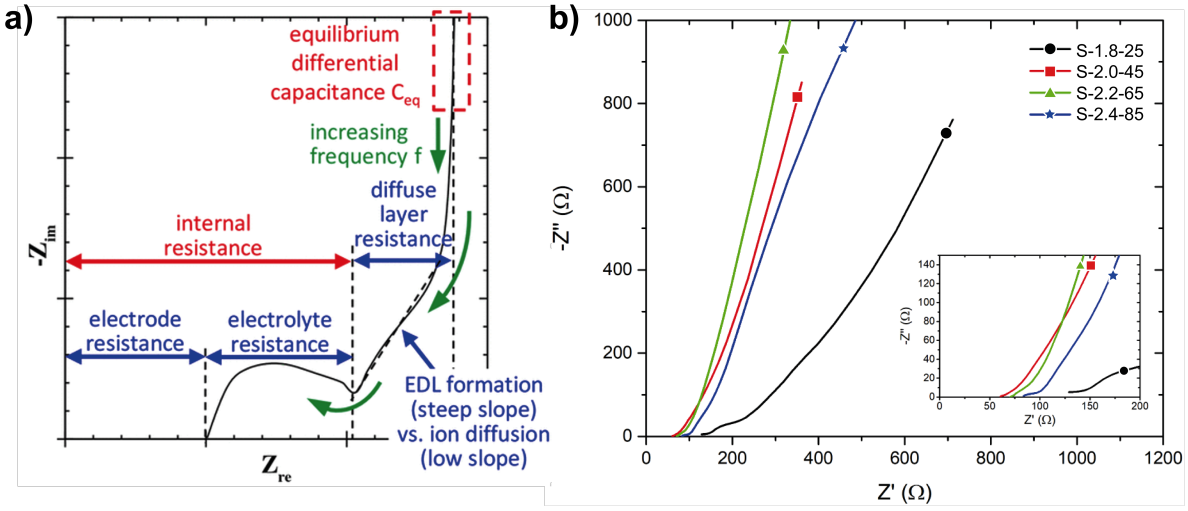

Figure 31: EIS characterization of the LIG microsupercapacitors. (a) Simplified reading of main supercapacitor parameters from a Nyquist plot, without reconstructing an equivalent circuit model. Taken from [186] (b) Electrochemical Impedance Spectroscopy Nyquist plot of the four main samples. The inset shows the EIS data at high frequencies. Symbols have been added for accessibility purposes only.

Now, going back to the initial focus, the areal capacitances of all eight LIG MSC devices have been plotted against the main laser parameters in Figure 32 (a, b, c), to graphically

show their influence in fabricating the best performing LIG microsupercapacitors. These dots are the average value of multiple samples fabricated at each condition, to account for device-to-device variability.

In Figure 32a, the areal capacitance is plotted against the laser power. The first observed feature is that the pairs of samples fabricated at the same power render very similar capacitance results, regardless of its scan speed at which they were fabricated. Figure 32b does not show a clear correlation between the scan speed used and the capacitance achieved, which hints at the laser power being the most relevant parameter. This is further confirmed by Figure 32c. The laser fluence is the irradiated energy per unit area by the laser, a parameter calculated directly from the laser parameters, and many studies present it as the governing parameter of the laser writing material transformation. However, in this study, its influence is not very clear. The conditions with the lowest fluence, S-2.2-80 and S-2.4-85, are in the lowest capacitance range, as are S-2.2-65 and S-2.4-70, which also have a fluence lower than 50 J/cm^2. However, S-2.0-60, which has an even lower fluence than those mentioned prior, showed a 40% higher capacitance. The highest capacitances were found in the lowest power samples, those manufactured at 1.8 and 2 W.

These results coincide with the insights taken from the characterization of the LIG materials. Regarding the material's microstructure as seen by SEM, S-2.0-45 was the most homogeneous sample and showed the best porosity distribution, as it had more and smaller pores of around 2.5 μm, in contrast with the bigger pores of the higher power samples. S-2.0-45 also presented the highest graphenic quality at the center of each raster line, according to the Raman spectroscopy mapping. It also showed the lowest I_D/I_G ratio and the highest I_{2D}/I_G ratio of all four samples, confirming the presence of low-defective multilayer graphene nanoflakes forming a conductive network. S-2.0-45 reached a maximum capacitance of 22.2 mF/cm^2 at 0.05 mA/cm^2, which is one of the highest values reported in the literature for an all-carbon LIG MSC.

In order to compare the performance of supercapacitors in terms of its energy and power densities, the Ragone plot, introduced before, is the representation of choice. In Figure 32d, sample S-2.0-45 (in red) is compared with many other LIG microsupercapacitors. The included devices have not been complemented by pseudocapacitive materials, doped with heteroatoms or any other strategy that involves compositing the LIG material. The device presented in this work reached 3.07 μWh/cm^2 and 0.0462 mW/cm^2 at 0.05 mA/cm^2, which is higher than similar devices in the literature, and even surpasses those doped with N or B atoms [187], [188]. The

energy density decreased down to 1.18 µWh/cm² at 0.5 mA/cm², which is 40% less than the measurements found at the lowest current density. But even with this decrease, steeper than other mentioned devices, the results are very competitive in the field.

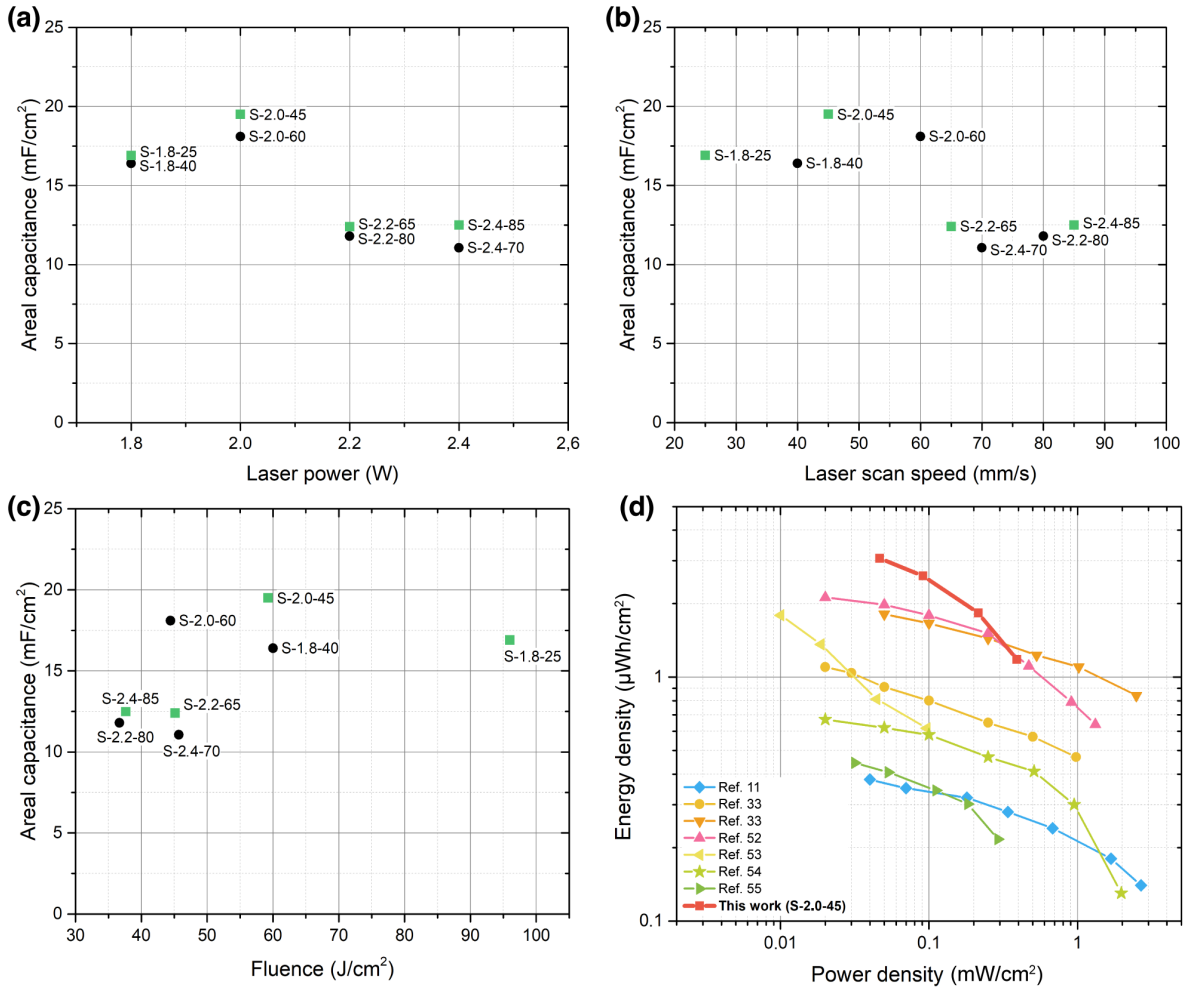

Figure 32: Areal capacitance versus main laser parameters, and Ragone plot. Areal capacitance of the measured microsupercapacitors in the 1M H_2SO_4 PVA gel electrolyte at 0.1 mA/cm2, as a function of the main laser parameters: (a) laser power, (b) laser scan speed, and (c) laser fluence. The four samples of interest (mentioned in Figure 20) are marked as green squares. (d) Area-specific Ragone plot, including the device S-2.0-45 and similar devices from the literature. The references must be consulted at the original paper [176].

Finally, to explore the durability of the device, cyclability measurements are performed, where a large number of charge-discharge cycles are done at a high current density, to resemble normal operation. In Figure 33 the capacitance retention of the device is shown, relative to the capacitance measured for the first cycle. A fast decrease of around 10% happens in the first 250-300 cycles, and after that, the capacitance only decreases almost linearly an extra 6% for the following 1700 cycles. At 2000 cycles, the

capacitance retention is 84%. This result can be easily improved by strategies such as pre-cycling of the device, as for industrial applications, even if the device properties are a bit worse, they should keep constant for as long as possible during normal operation.

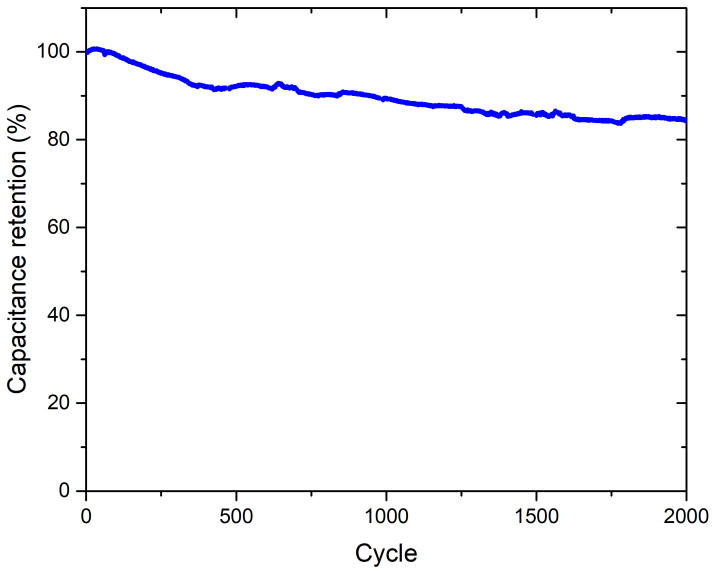

Figure 33: Capacitance retention after 2000 charge/discharge cycles at 0.2 mA/cm² of S-2.0-45.

One last parameter that has great effect on the areal performance of these microsupercapacitors, and that has not been mentioned yet, is the thickness of the fabricated carbon material. Every LIG sample mentioned in this thesis has been fabricated on 60 µm thick polyimide tape, coated with an adhesive layer. This is however not the norm in the research field, where most of the studies are performed starting from 125-127 µm thick films. According to these studies, the final thickness of LIG material they could achieve was in every case of around 50 µm [53], [89], [188]–[196]. By using 60 µm polyimide tape placed on an external support, microsupercapacitors are fabricated reaching a much higher active material to total volume ratio, while achieving the same 50 µm of LIG, reducing the total volume of wasted material.

This has implications in sustainability, as less waste is produced, but it has even more advantages in terms of its integration. Apart from the lateral miniaturization of dimensions, the shrinking of the thickness of these devices maximizes its ability to better adapt to the mechanical loads they could be subject to, and to be more conformal to the required bending conditions. On top of that, the smaller dimensions of these thin devices allow for much better stacking of devices in compact modules with higher

voltage or higher current configurations, depending if the stacked devices are connected in series or in parallel, respectively. These thin and small packages could be easily implemented on the skin or clothing of the users in a non-intrusive and comfortable way.

4.3. Higher voltage supercapacitor configurations

As introduced above, in order to integrate supercapacitors as power devices in everyday electronic applications, the voltage output that can be obtained from such devices is a key element. For example, to power a single LED, a voltage difference of between 1.8 V and up to 3.2 V must be applied, depending mainly on the color of the LED. This is even more obvious when looking at most consumer electronic platforms, which run at voltages of 3.3 V, 5 V, 9 V or 12 V, depending on the application. The selection of such voltages was just a requirement emerging from the breakdown voltage limit of the silicon scaling level of the processor at stake. With reducing gate dimensions, the voltage had to be reduced to avoid failures, although now other strategies are also in place, such as the use of high-k dielectrics. There is also a market effect in the process to settle on those "voltage steps". Standardizing components such as the USB port, rated for 5 V power delivery, influenced many designs in the portable electronics industry, similarly to what happened in the automobile industry, where the power supply is a 12 V lead-acid battery since many years.

As part of the DIGRAFEN and REGRAP-2D projects, one of the key objectives of the projects was to assemble an electronic interface between a solar cell and a supercapacitor, in order to make a small, self-contained, autonomous power unit that could be connected to an external sensor o to some communications platform. The solar cell would provide power to charge the supercapacitor, through the charging interface, which will give back the power when needed, to an external circuit/item. The system would run at 3.3 V, although it could be reduced according to the project development.

However, for the devices presented in the previous section, its operating voltage window is limited to 1 V by the selected electrolyte. Actually, aqueous-based gel electrolytes start to decompose once a 1.1 V voltage is reached. Therefore, the most obvious choice for increasing the voltage rating of a supercapacitor is to change the electrolyte choice into another one that can handle higher voltages. Both organic electrolytes or ionic liquids are able to withstand voltages of around 2.5 to 3.5 V in optimized conditions, with some ionic liquids reaching 4 V and beyond.

Such voltage can only be attained in ideal conditions, that is, the environment to which the electrolyte is exposed during operation must be completely free of water and other reactive contaminants. Achieving environments that are extremely water free is very challenging on earth, and special equipment (glove boxes) are designed to assemble and store such chemicals. Water and oxygen contents of around 2 parts per million (ppm) can be achieved in standard research-grade gloveboxes, where the supercapacitor is assembled and sealed completely before taking it out of the glovebox. Most of the times, due to the challenge that this presents, the devices are measured directly inside the same glovebox environment, to avoid contamination.

This procedure is extremely time consuming, requiring very expensive equipment that is difficult to scale to high-throughput industrial settlements. Furthermore, organic electrolytes and ionic liquids suffer from other issues that reduce its potential as supercapacitor electrolyte. For organic electrolytes, the large size of the ions involved increases their resistance and reduces the capacitance, as the smaller pores of the material cannot be reached. Ionic liquids, aside from being more expensive, also present a high viscosity, which increases its internal resistance. Apart from that, it is important to note that organic electrolytes are already being used in the industry, and that the interest in ionic liquids is high and growing, as the advantages are many and the issues are being mitigated.

On the other hand, changing the electrolyte is not the only option. In fact, a much more pragmatic approach can be taken to fabricate supercapacitors with "on-demand" voltage and current characteristics. By connecting in series and in parallel individual 1 V supercapacitors, both the current and the voltage can be increased to reach the required values. This can be done by connecting them through external circuitry, although an increase in the internal resistance can be expected. As a first demonstration, we connected nine individual devices, in a 3x3 configuration (three MSCs in series, and three of those units in parallel) to power a green LED successfully for over a minute. The device, shown in Figure 34, reached a maximum voltage of 3 V.

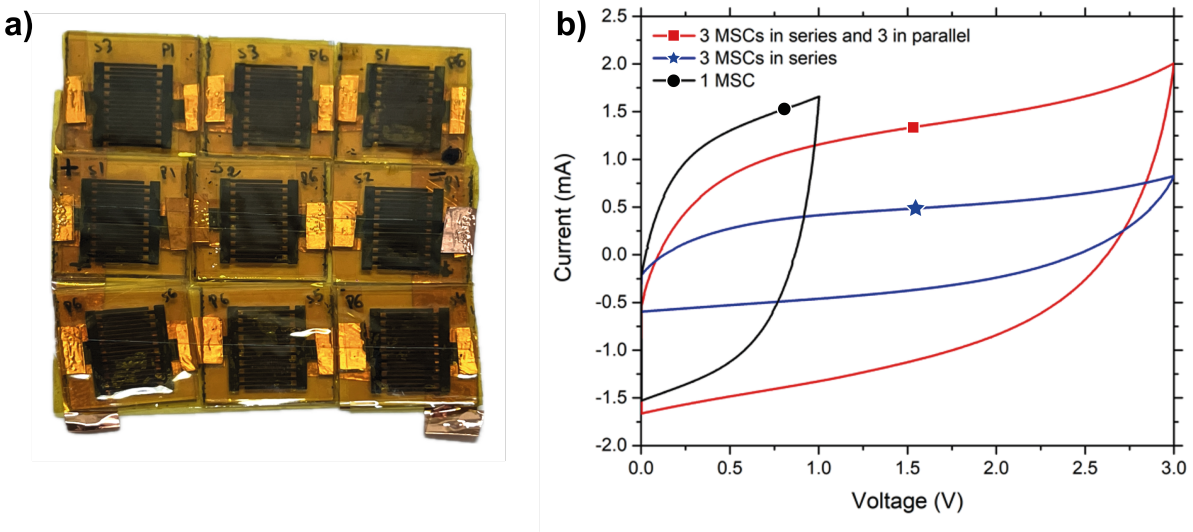

Figure 34: Electrochemical characterization of a high voltage supercapacitor. (a) Picture of the fabricated 3x3 device, with individual microsupercapacitors connected through copper tape. (b) Cyclic voltammetry at 0.1 V/s scan rate of the different supercapacitor arrangements, one single device, a connection of three in series and the full 3x3 device. Symbols have been added for accessibility purposes only.

On the other hand, a smarter approach can be taken by exploiting the advantages of direct laser writing. As the technique is very flexible, the geometry of the fabricated devices can be easily changed just by loading a new vector design in the software program. This way, the electrical connections of the devices in series previously made with copper, now can be directly built using the same LIG material, as seen in Figure 35. By connecting electrodes laterally, the string of supercapacitors will now behave as a single unit, extending its voltage range as far as the number of 1 V supercapacitors included.

However, if the electrolyte is extended through the entire surface of the device, touching several individual MSCs, the voltage advantage disappears. Each individual supercapacitor should be ionically isolated from the rest, as the electrical conductivity of the electrolyte is not zero. One single "pool" of electrolyte will sense the increased voltage through the entire device, limiting again its use to a maximum of 1 V to avoid hydrogen and oxygen evolution reactions. Therefore, the individual devices must be assembled with care to separate the electrolyte regions to the interdigitated area of each individual supercapacitor.

By using a gel electrolyte, assembling this device gets a bit easier as the viscosity helps contain the electrolyte to its intended area. Simply by using small ribbons of polyimide tape, the separations between devices can be placed, isolating and dividing the electrolyte into the individual devices below. Other materials can also be used to

separate the electrolyte in case polyimide is not enough. For example, if using liquid electrolytes (aqueous or other kind), a bi-component epoxy glue can be used, as it can be conformed into narrow strings and placed along the separation lines.

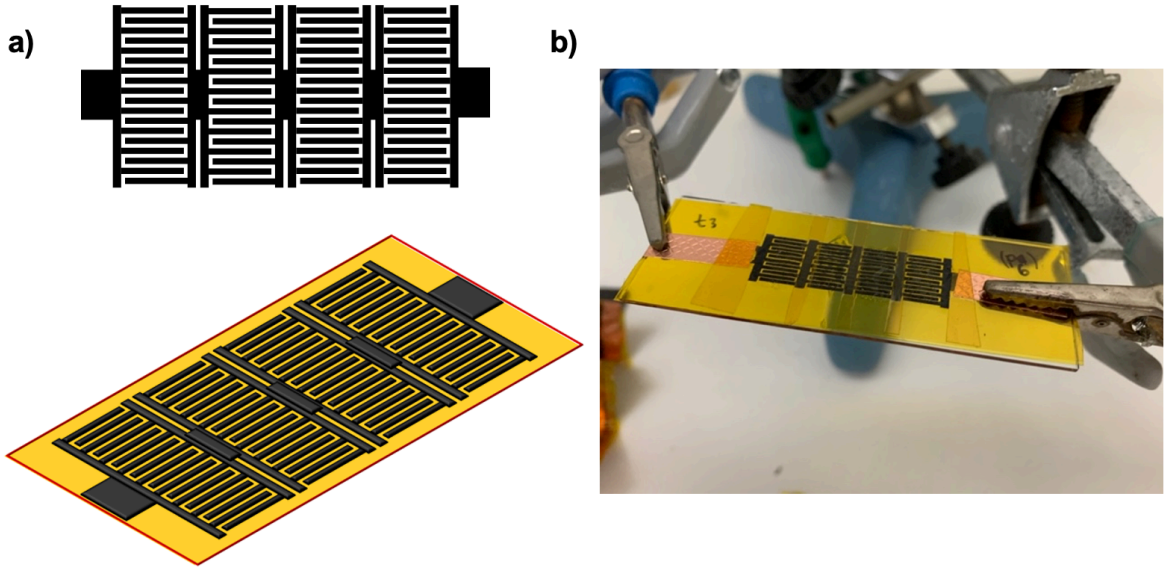

Figure 35: Integrated high voltage microsupercapacitors. (a) Design of the integrated 4x1 microsupercapacitor to be fabricated by laser writing and its 3D representation on a polyimide film. (b) Picture of the fabricated version of the design, connected to the external characterization setup through crocodile clips. The vertical polyimide strips can be seen, including two more to protect the copper contacts.

In order to achieve a 3.3 V output, as was required by the project, four supercapacitors should be assembled in series. In Figure 35 the first design proposed and fabricated is shown.

However, in order to make it fit into the fabricated electronic board, the design was slightly modified. In this version of the electronic board, the space allocated for the supercapacitor was restricted to a fraction of the total area, on one side of the board. The design process is very flexible, and the polyimide film can even be cut to size using a higher power along the outline path, as shown in Figure 36.

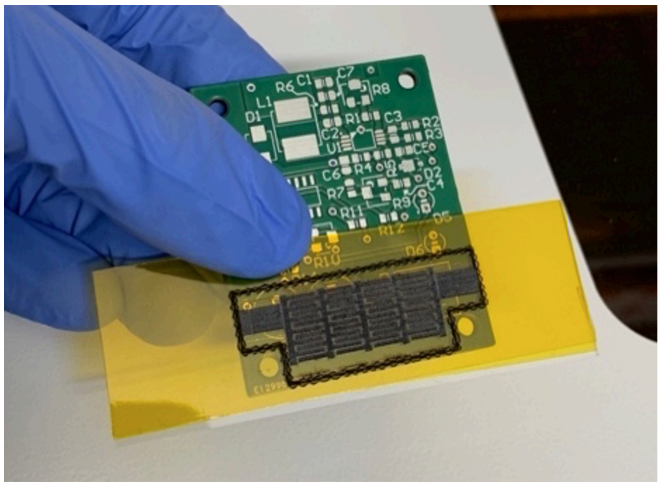

Figure 36: 4x1 microsupercapacitor, superimposed on the prototype electrical board, checking the fit of the MSC outline on the real device.

Regarding the electrochemical performance of such device, Figure 37 shows the CV and GCD of one of such microsupercapacitors, with four devices connected in series. The device reaches easily 3.3 V without any abnormal increase in current, and it could even reach a maximum of 4 V. However, the current levels for only one device are very low, not enough to be integrated together with a solar cell. Therefore, using the thin structure of the polyimide substrate and the fabricated device, connections in parallel are made, placing one device on top of the next one and connecting the contacts using adhesive copper tape. In Figure 38, the CV plot of one device is shown in red, which amplitude gets almost duplicated when two of them are connected in parallel. The final device, plotted in green, is the parallel connection of eight modules of four microsupercapacitors each, able to charge and discharge reliably at 5 mA.

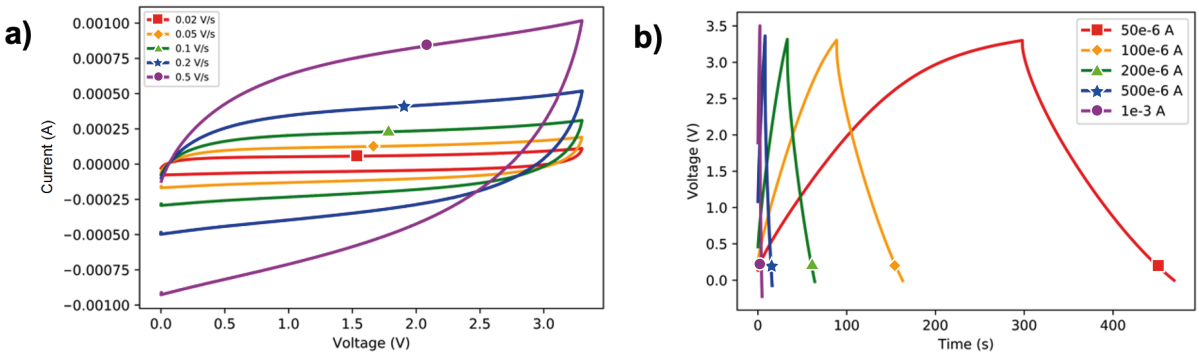

Figure 37: Electrochemical characterization of one 4x1 MSC device, reaching 3.3 V. (a) CV measurement at scan rates ranging from 0.02 V/s to 0.5 V/s in a voltage window of up to 3.3 V. (b) GCD measurement at currents from 0.05 mA to 1 mA. Symbols have been added for accessibility purposes only.

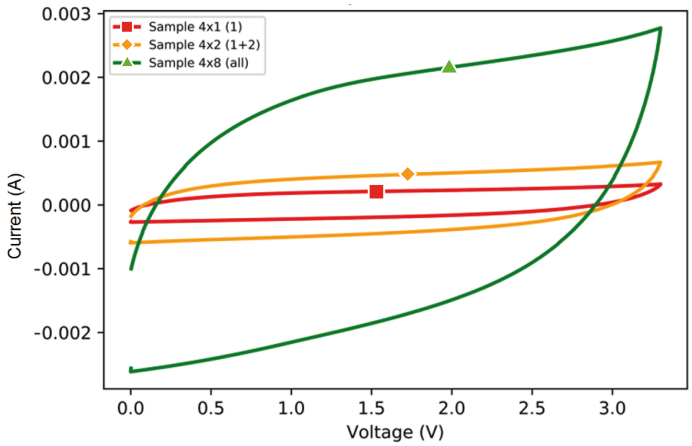

Figure 38: Cyclic voltammetry measurement of high voltage devices connected in parallel. All at 0.1 V/s scan rate: one module of four MSCs connected in series (red), two of such modules connected in parallel (yellow) and eight of the same modules connected in parallel (green). Symbols have been added for accessibility purposes only.

The full device had an ESR of 110 ohms and a capacitance of 30.5 mF with a high energy density, thanks to the extended voltage, of 89.9 µWh, at 0.2 mA. At that current, the power is 0.65 mW. As regular supercapacitors get their metrics normalized by the weight, area or volume, taking into account the area of the device, of 12 cm^2, the previous values are put into context. The capacitance of the device gets reduced, reaching 5.09 mF/cm^2, but the real increase comes in energy density, at 7.49 $\mu Wh/cm^2$ with a power density of 0.054 mW/cm^2. The maximum power is measured to be 0.976 mW/cm^2 at 5 mA, retaining a decent energy density of 1.63 $\mu Wh/cm^2$.

As a final prototype, once the printed circuit board (PCB) got its final dimensions, greatly reduced from the previous iteration, a high voltage supercapacitor device was fabricated with the main task of maximizing current as much as possible, as the solar cell delivers more current that what the supercapacitor could manage. This way, after experimenting with interdigitated electrodes made on thicker flexible polyimide (125 µm) as seen in Figure 39, the design was settled on sandwich supercapacitors. These devices have been mentioned only briefly in the beginning of this thesis, and consist of continuous thin film electrodes, which are assembled in pairs, face to face and in close contact, but electrically insulated through a separator. The separator can be any membrane that allows for ionic conductivity while insulating the electrodes electrically, and for assembling this device, standard filter paper has been used.

Figure 39: Examples of 2 V supercapacitor modules. (a) 2 V microsupercapacitors separated with an epoxy string. (b) 2 V microsupercapacitors separated with a polyimide film.

While the normalized electrochemical properties of interdigitated electrodes are indeed better when compared to sandwich supercapacitors, this happens because only the active carbon area is taken into account. However, the interfinger gap does not contribute to the active area, but it is needed for the correct functioning of the device. The space it takes, around 40% of the total area in Figure 17b, can be used as active electrode area if a sandwich configuration is used, where the lateral gap is replaced by a vertical gap in the z direction. This way, a trial using bulkier, continuous electrodes was proposed. The strategy to achieve higher voltage is the same, but now all the individual supercapacitors should be connected through external wiring. As the new board required 2 V of delivered voltage, instead of four devices in series, now with two is enough. The final assembled device, shown in Figure 40, is formed out of three modules connected in parallel, each having two supercapacitors connected in series.

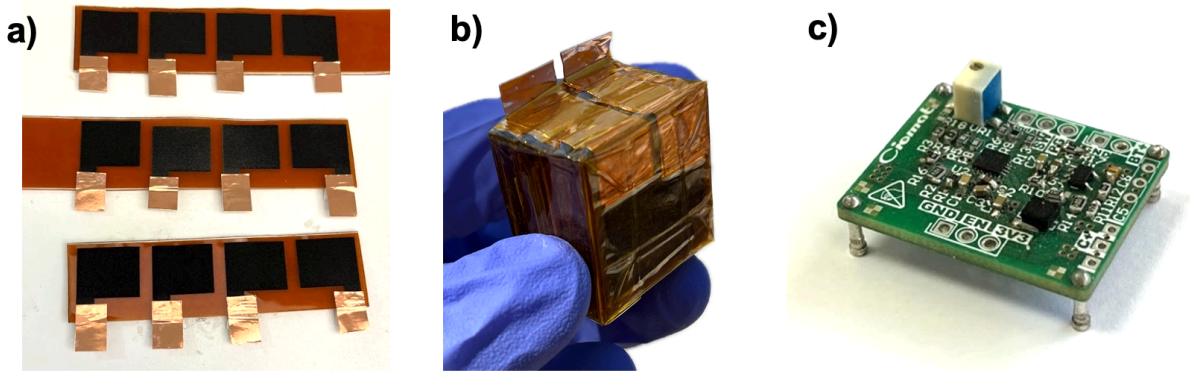

Figure 40: Final 2V supercapacitor prototype and board. (a) Fabricated thin film continuous LIG electrodes to assemble sandwich supercapacitors. (b) Picture of the fabricated 2 V sandwich supercapacitor in a 2x3 configuration, encapsulated and with the contacts prepared for its integration in the PCB board. (c) Final design of the PCB board.

Thanks to the larger area of this device, and the slight pressure that the encapsulation applied to the structure, the electrochemical performance of the device met the requirements. The device presented a low ESR of only 36 Ω, with a total capacitance of

66.6 mF at 1mA. Even at 10 mA, the device maintains a capacitance of 36 mF. Although the lower voltage window, the energy density is still very high at 68.9 µWh at 1 mA, with a high power of 14 mW. The encapsulated device is a very capable supercapacitor which will be integrated in the final prototype for the project.

Only for comparison, normalizing these values by the actual used carbon area of the device, which is higher than in the previous prototype, we conclude that the sandwich configuration uses less effectively the material. The areal capacitance reaches 3.44 mF/cm^2 once the total area is taken into account, with a maximum energy density of 17.8 µWh/cm^2 and a maximum power density of 0.37 mW/cm^2.

Figure 41 presents the characterization performed between 0 and 2 V of the full sandwich device, showing a CV measurement reaching high current values and very symmetric, a CGD profile which maintains the triangular shape and working fine at high currents, and an EIS Nyquist plot which corroborates the low ESR resistance.

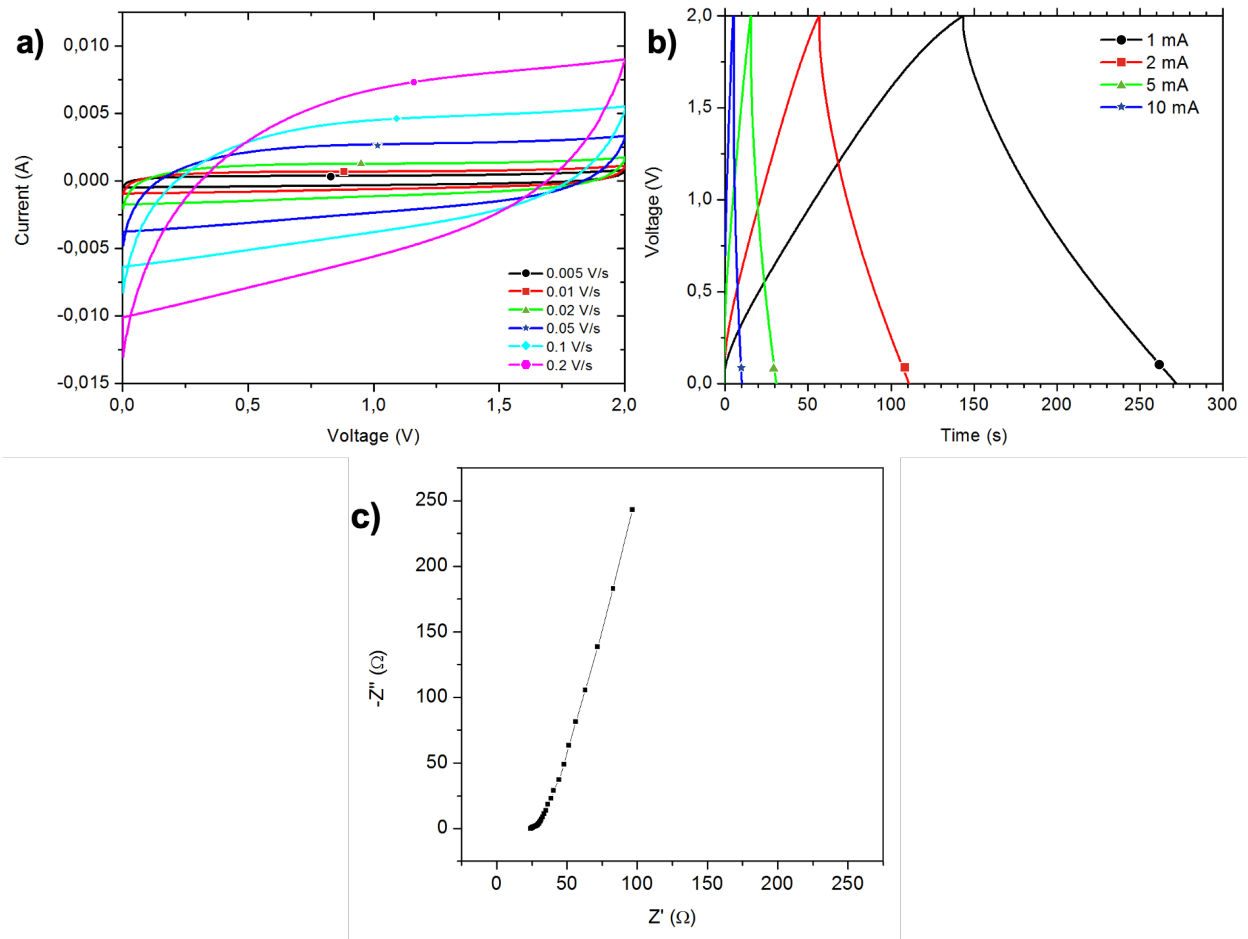

Figure 41: Electrochemical characterization of sandwich 3x2 LIG supercapacitor. (a) CV measurement at scan speeds from 0.005 V/s to 0.2 V/s, in a 2V voltage window. (b) GCD measurement at high currents, from 1 mA to 10 mA. (c) Nyquist plot of the device from EIS measurement.

4.4. Hybrid microsupercapacitors in ionic liquid electrolyte

The last section of this chapter on supercapacitors is dedicated to hybrid microsupercapacitors using heterostructures of LIG and molybdenum compounds, in ionic liquid electrolytes. This work was performed during two research stays carried out at CIRIMAT, a research institute located in Toulouse (France) dedicated to materials science research, ranging from ceramics, to surface treatments and electrochemistry. Electrochemistry research was performed within the RTS group (Revêtements et Traitments de Surface), under the direction of prof. Patrice Simon. The first research stay period was funded by the *Ministerio de Universidades* FPU program "Estancias Breves 2022" and was carried out from September to December 2022 (EST22/00614). After that period, in order to complement the results, a second, shorter stay was carried out at the same group for one extra month, from May to June 2023.

The most effective strategy to increase the performance of supercapacitors is compositing them with pseudocapacitive elements. As explained in previous sections, pseudocapacitance arises from elements in the electrode which are susceptible to carry on redox reactions at the surface. One example of such elements are metallic oxides, such as MnO_2, or Fe_2O_3.

As pseudocapacitance is a process arising from surface redox-reactions, starting from a 2D material precursor, like MoS_2, exfoliated into few-layer nanoparticles or nanosheets, could be ideal for this purpose. MoS_2 can be oxidized into molybdenum oxides, which are pseudocapacitive, given enough time and temperature [197]. Combining these two ideas, a UV laser has been used to locally heat a MoS_2 spray-coated layer on top of laser-induced graphene microsupercapacitors. The MoS_2 gets transformed into MoO_x, showing redox-activity and an increase in the total capacitance, energy, and power density. Using several MoS_2 solutions, exfoliated in different solvents and centrifugated at variable speeds, it is also expected to see a relation between the exfoliated nature of the MoS_2 solution (extracting a more exfoliated fraction for higher centrifugation speeds) and the redox response.

At this point, a comment must be made. Several factors affected the obtention of strong results for these experiments, limiting the conclusions to a first indicative demonstration of the research hypothesis. Despite facing challenges such as the difficulty of fixing the mass loading of Mo compounds on the samples, variable electrochemical performance in the used LIG MSCs, and time and technical constraints, we managed to achieve some encouraging positive results. As said before, they serve as the basis for future work in this topic.

4.4.1. Fabricated devices

Ten samples were fabricated and measured, all LIG MSC devices. As stated previously, the varying parameters for LIG fabrication are the laser power (W), the scan speed (mm/s) and the number of laser scans. MoS_2 solutions were prepared starting from MoS_2 powder (Sigma Aldrich) dispersed in mixtures of ethanol and water, sonicated for 8 h and centrifugated from 20 min at different speeds, keeping the supernatant fraction of the solution. The parameters used to identify the MoS_2 dispersions are then, ethanol percentage in the solvent (%) and centrifugation speed (rpm). Using the facilities of the electrochemical labs at CIRIMAT, all of them were measured in an EMIM-TFSI ionic liquid electrolyte in a voltage window from 0 to 2.5V. All of them had contacts made with sputtered Au, as shown in Figure 42, covered by conductive copper tape to get a more rugged, durable contact. All of them had the same interdigitated geometry, and the total sample size fitted the dimensions of the UV laser chamber. The different MoS_2 dispersions were spray coated on the LIG MSCs, monitoring its mass using a microbalance (Sartorius).

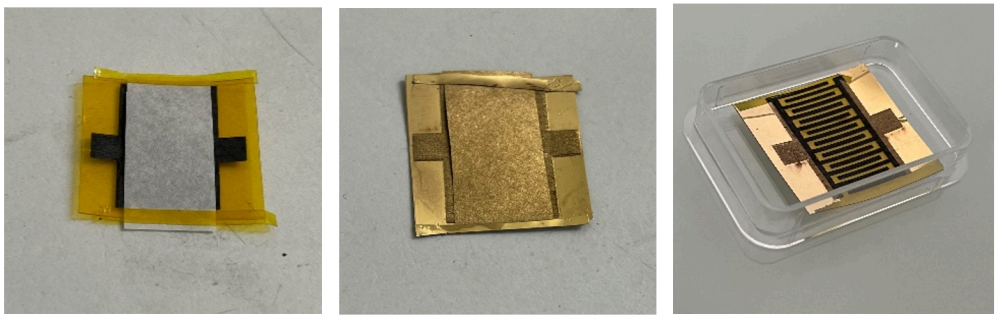

Figure 42: Fabrication process of the sputtered gold contacts on the LIG MSC using a hard paper mask to protect the interdigitated area.

Two samples were made and measured in an initial experiment. For these samples, LIG was made at 2.2 W 60 mm/s using a single laser pass, on 125 µm thick polyimide film. These parameters were selected after further optimization of the LIG material on thicker polyimide substrates, which could take higher powers without structural degradation. A bare LIG MSC with no MoS_2 is named S1, and a LIG MSC device complemented with MoS_2 (80% 0 rpm), S2.

For the samples made in the second experiment, LIG was made at 2.4W 80mm/s using two laser passes, following an optimized recipe from our group. The polyimide substrate used was the same, 125 µm thick flexible polyimide. The MoS_2 deposited on the LIG MSC samples was exfoliated at different conditions, both in the solvent and in the centrifugation process, indicated in Table 2.

		Ethanol % in solvent	
		40 % EtOH	**80% EtOH**
Centrifugation speed	**0 rpm**	S3 (40_0)	S7 (80_0)
	1000 rpm	S4 (40_1000)	S8 (80_1000)
	3000 rpm	S5 (40_3000)	S9 (80_3000)
	5000 rpm	S6 (40_5000)	S10 (80_5000)

Table 2: MoS_2 liquid phase exfoliation conditions and sample naming scheme.

After this, all MoS_2 samples were laser treated with a UV laser (405 nm) at 18% power (100% being 150 mW), 10 mm/s scan speed, within a closed chamber with small air flow. The design was tailored to overlap exactly the existing interdigitated design. Only the LIG area was lasered, leaving the gap in between electrodes unexposed. XRD was performed to check the transformation of MoS_2 into molybdenum oxides.

In Figure 43, insights on the laser oxidation of MoS_2 are provided. In figure a, the black line represents the spectra of the as-deposited MoS_2, while the red line corresponds to the laser-processed sample. The vertical lines in Figure 43a mark the position of the MoO_2 specific peaks in the XRD spectra. Figure 43b, on the right, shows the initial laser trials performed to select the optimal laser conditions for MoS_2 oxidation, showing the transformation of the grey MoS_2 material into a blueish material corresponding to molybdenum oxide.

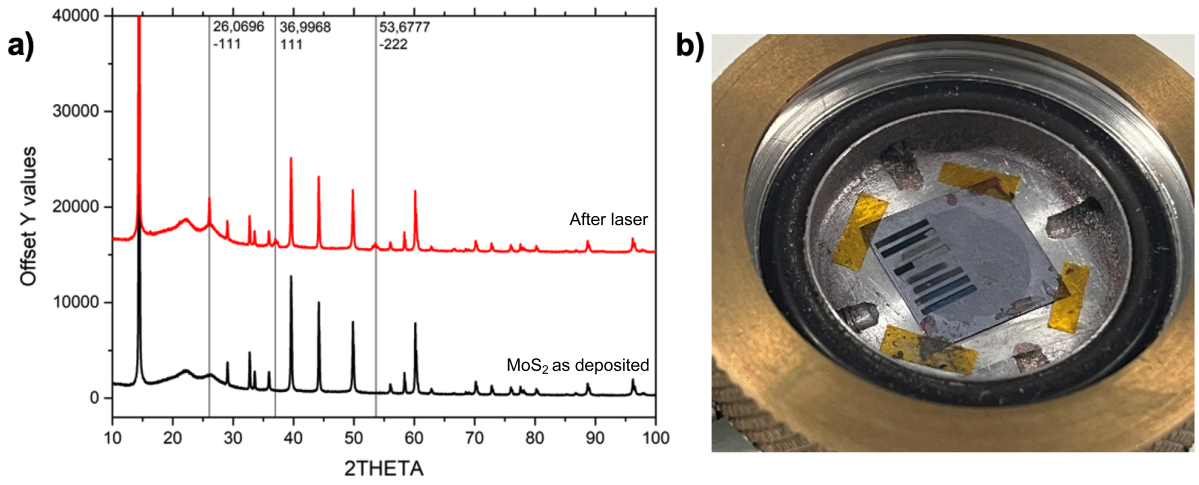

Figure 43: XRD characterization of the MoS_2 before and after laser exposure. (a) XRD spectra of a LIG/MoS_2 sample before laser exposure (black) and after laser exposure (red). The XRD signature for MoO_2 is marked with vertical lines according to JCPDS card #86-0135. (b) Initial trials of MoO_x formation through laser oxidation, on a MoS_2 sample drop casted on polyimide. The sample is in a chamber with forced airflow.

4.4.2. Electrochemical characterization

As this experiment was performed in two stages, first the results obtained in the first period are shown, in Figure 44 and Figure 45. Figure 44a presents the CV characterization of a LIG microsupercapacitor measured at CIRIMAT in pure EMIM-TFSI electrolyte (up to 2.5 V). The achieved currents are low, and some degradation "shoulders" that can be attributed to small amounts of water and oxygen, can be seen above 2 V. For Figure 44b, the same data is presented using an inverted plot, where each CV current density is normalized by its scan rate, achieving units of $mC/V \cdot cm^2$. This helps to visualize the effect that faster scan rates have on the electrochemical response of the sample, such as redox process that can be diffusion limited.

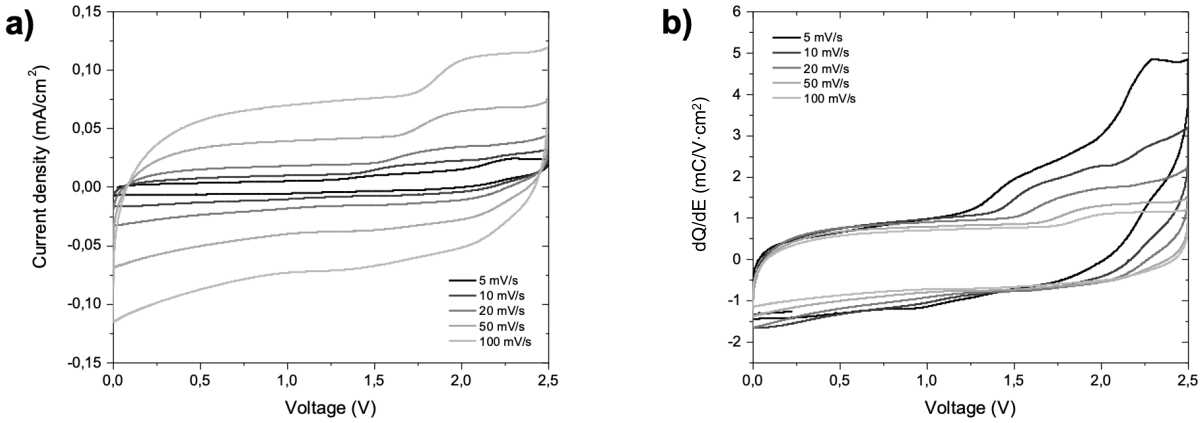

Figure 44: Electrochemical characterization of S1, a bare LIG MSC (no MoS2) measured in pure EMIM-TFSI ionic liquid electrolyte. Cyclic voltammetry (CV), both as (a) current vs potential, (b) dQ/dE vs potential

Figure 45 shows the CV measurement of a S2, LIG MSC complemented with spray coated MoS_2 exfoliated in 80% EtOH solvent with no centrifugation. The MoS_2 material, after laser exposure, was partially transformed in MoO_2 and therefore some redox peaks appear in the CV.

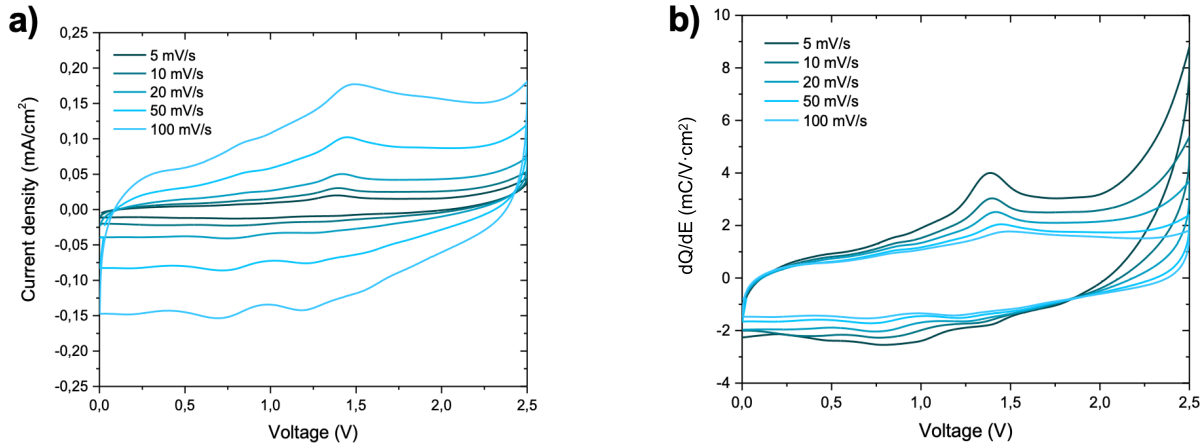

Figure 45: Electrochemical characterization of S2, LIG MSC with lasered MoS_2 (80% EtOH, 0 rpm) measured in pure EMIM-TFSI electrolyte. Cyclic voltammetry, both as (a) current vs potential, (b) dQ/dE vs potential.

While the current of this device is still low, a clear increase can be seen compared with the bare LIG device (S1). Comparing both in Figure 46, redox peaks can be appreciated both in the charge and the discharge cycles.

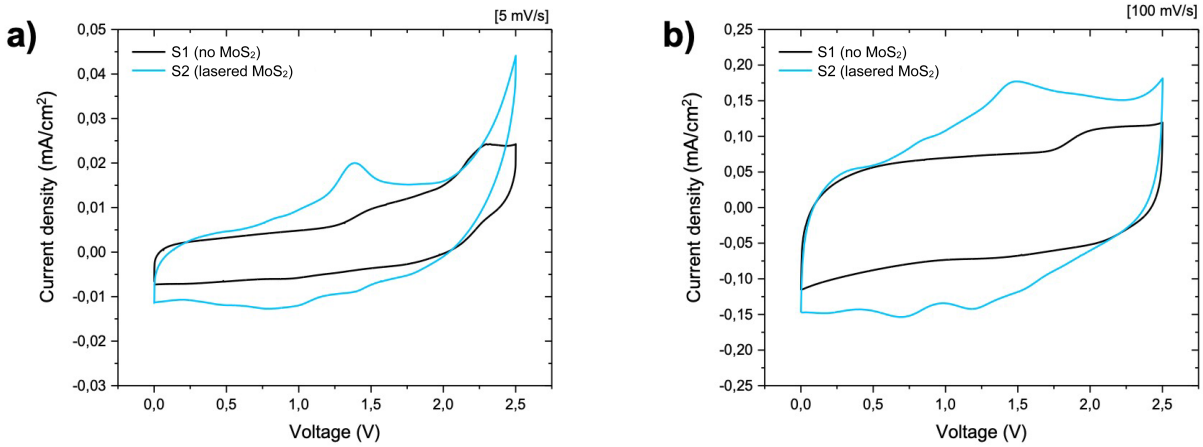

Figure 46: Comparison of device S1 (without MoS_2) and device S2 (with laser proceszed MoS_2) CVs at (a) 5 mV/s, and (b) 100 mV/s.

After this result, it was decided to dive deeper into the electrochemical properties of MoS_2 and MoO_x fabricating more devices and exploring different conditions. Eight MoS_2 dispersions were produced, with different exfoliation regimes (using two solvents) and different centrifugation speeds, to test the influence of the exfoliation degree and fraction of few-layered nanoparticles content on the electrochemical activity.